IEEE Access
Multidisciplinary ⋮ Rapid Review ⋮ Open Access Journal

Received 23 August 2022, accepted 5 September 2022, date of publication 8 September 2022, date of current version 16 September 2022.

Digital Object Identifier 10.1109/ACCESS.2022.3205320

RESEARCH ARTICLE

ZnO Film Flexible Printed Circuit Board pH Sensor Measurement and Characterization

PO-HUI YANG, (Member, IEEE), CHE-TSUNG CHAN, AND YING-SHENG ZHANG
Graduate School of Electronic Engineering, National Yunlin University of Science and Technology, Douliou 64002, Taiwan
Corresponding author: Po-Hui Yang (phyang@yuntech.edu.tw)

ABSTRACT An electrochemical zinc oxide (ZnO) pH sensor is proposed and prototyped using a flexible printed circuit board (FPCB). The device is resistant to acidic and alkaline solutions and exhibits excellent electrical conductivity. The sensing film was deposited by radio-frequency sputtering, providing a dense ZnO layer, and (3-aminopropyl)triethoxysilane (APTES) was used to enhance the chemical stability of the ZnO in acidic solutions. The proposed pH sensor has an average sensitivity of 37.52 mV/pH, linearity of 0.995, and a repeatable RSD value of 2.4%. Testing was conducted with Carmody's buffer pH 2-10 and a voltage-time measurement system. The stability of the prototype was determined by the measurement of the drift and hysteresis effects.

INDEX TERMS pH sensor, biosensor, zinc oxide (ZnO), flexible printed circuit board (FPCB).

I. INTRODUCTION

pH sensors are used in various fields such as environmental analysis, clinical diagnostics, and effect on enzyme activity. The fundamental H^+ ion plays an essential role in most enzymatic biosensors. Meanwhile, other sensing methods have also been proposed, such as optical pH sensing [1], SPR/LSPR optical sensor [2], [3], [4], [5], [6], [7], [8], [9], [10], [11], [12], voltammetry sensor [13], electrochemical sensor, and EGFET sensor [14].

In many pH sensing materials, zinc oxide (ZnO) has the characteristics that make it particularly advantageous, such as a wide band gap (3.37 eV), high excitation binding energy (60 meV), room temperature stability, non-toxicity, low cost, and its tendency to be an n-type semiconductor. This makes ZnO a clear choice for biosensors [15], but there are drawbacks; for example, ZnO tends to dissolve slightly in acidic or alkaline solutions. Especially when it is used as a pH sensing material, it dissolves rapidly below pH 3.8 [16] yet is relatively stable when pH is neutral (pH 7) [17]. If the dissolution problem can be mitigated, ZnO would be a suitable amphoteric oxide for use in acidic and alkali solutions. In the past, researchers developing prototypes protected the sensing layer using a doping material. Studies are showing this being done with Al [18], Mg [19], and Pd [20], and some have used a proton exchange film (3-aminopropyl)triethoxysilane (APTES) modified with ZnO [21]. APTES can build aminosilane layers to protect the ZnO from the acid dissolution process, which depends on the ZnO material's shape, thickness, and fabrication method. There are several alternate fabrication methods for ZnO sensors, such as sol-gel [22], hydrothermal [23], sputtering [24], [25] and atomic layer deposition (ALD) [26], resulting in ZnO with different surface morphologies. Considering the ease of fabrication and adhesion quality, we use sputtering to fabricate ZnO thin films.

A flexible pH sensor substrate is a reasonable choice when constructing a comprehensive industrial and biomedical sensor. Flexible substrates in the literature are commonly PET (polyethylene terephthalate) [27], paper [28], or PI (polyimide) [29]. PET substrates have the advantage of being lightweight but have unsatisfactory temperature tolerance. Paper substrates are low-cost but are susceptible to moisture effects. Compared to PET and paper substrates, PI substrates have better temperature resistance, chemical stability, mechanical properties, and excellent dielectric properties. PI is the most commonly used substrate material for Flexible Printed Circuit Board (FPCB). In addition, the standard FPCB process accommodates copper traces and electroless nickel immersion gold (ENIG) layers [30]. Using ENIG improves chemical stability in various pH buffer solutions.

The associate editor coordinating the review of this manuscript and approving it for publication was Santosh Kumar.

Therefore, for this study, the sensing film pattern was first fabricated using the established FPCB process, after which a dense layer of ZnO was deposited using radio frequency (RF) sputtering. The pH sensor in this study utilized the potentiometric measurement [31] of an extended gate field effect transistor (EGFET) [32]. This signal was fed to an instrumentation amplifier (INA), after which it was possible to test the performance of the device.

II. EXPERIMENTAL

A. MATERIAL

A radio frequency sputtering system fabricates our ZnO sensing film. The pH sensor substrate is FPCB, manufactured by Ruixing Circuit Co., Ltd. (China). The ZnO targets were purchased from Ultimate Materials Technology Co., Ltd. (Taiwan). The buffer solution composed in this experiment is the citric acid powder (purchased from J.T. Baker Corp. (USA)), boric acid powder (purchased from Katayama Chemical Co., Ltd. (Japan)), trisodium phosphate powder (purchased from Japan), four Plus Chemical Co., Ltd. (Japan)). The protective layer of our pH sensor is APTES, sold from Sigma-Aldrich Co. (USA).

B. PREPARATION OF THE PH SOLUTION

A comprehensive pH range buffer solution was prepared following the system established by Walter R. Carmody [33]. Carmody solution is easily prepared and precise and is considered a wide-range buffer solution. The pH range of the buffer solution was 2.0 to 12.0, requiring only two stock solutions mixed with three common chemical materials. Solution "A" used boric acid 0.20 M, citric acid 0.05 M, and solution "B" used sodium phosphate tribasic dodecahydrate 0.1 M. A pH meter and test paper were used to ensure the pH was correct. Table 1 shows the mixing ratios of solutions A and B.

TABLE 1. Carmody buffer solution mixing ratio.

Buffer Solution (pH)	Solution "A" (mL)	Solution "B" (mL)
02.0	48.75	01.25
04.0	38.75	11.25
06.0	29.50	20.50
08.0	21.25	28.75
10.0	13.50	36.50
12.0	04.25	45.75

C. FABRICATION OF THE FPCB SENSOR

FPCB was selected as the sensor substrate for this study due to its flexibility, durability, and thinness [34]. The standard single-sided FPCB process was used in manufacturing. Figure 1(a) shows a cross-section of the FPCB sensor. The first layer was PI, which exhibited high mechanical strength and chemical resistance and could tolerate a wide temperature range. The second layer was copper traces, highly conductive and resistant to twists and turns. The third layer was also PI but had open electrode windows to the copper layer below. An upper surface using ENIG was applied to the open windows to prevent the copper traces from oxidizing.

Figure 1(b) is a plan view of the 30 × 35 mm FPCB sensor. It houses six working electrodes, each with a diameter of 2 mm, and the structure for these was APTES/ZnO/Au/Ni/Cu/PI. The outer electrode windows functioned as reference electrodes and solution ground windows. The reference electrode was used to provide a steady ground potential, which, according to the LT1167 INA datasheet, indicates it can be used reliably to generate an INA input bias current return path.

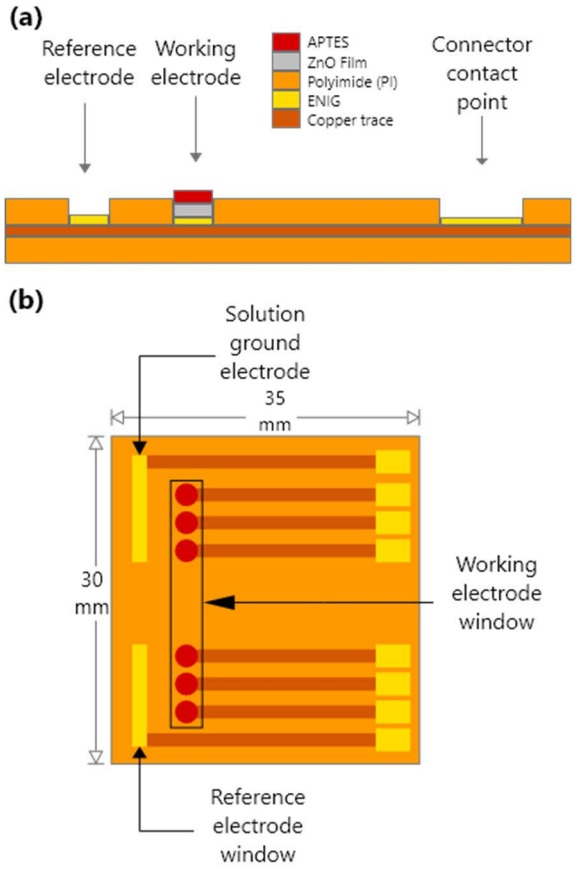

FIGURE 1. (a) Cross-section of the FPCB sensor, and (b) Top view of the FPCB sensor.

D. FABRICATION OF THE ZNO SENSING FILM

The ZnO target (99%) was deposited on the working electrode of the FPCB film by RF sputtering. Table 2 shows the ZnO film sputtering parameters where RF power was 60 W, Gas pressure was three mTorr, the argon to oxygen ratio was 9 to 1 (sccm), and a deposition time of 60 minutes was allowed to obtain a ZnO film with a thickness of 155 nm.

E. FABRICATION OF THE APTES MODIFIED LAYER

Drop-casting [35] was used to modify the ZnO layer by APTES. 2 μL of APTES (99 wt%) solution was dropped on

TABLE 2. ZnO film sputtering parameters.

Film thickness	Gas flow ratio (Ar: O2)	RF power	Deposition pressure	Deposition time
155 nm	9:1 (sccm)	60W	3 mTorr	60 minutes

the working electrode windows twice and diluted to 1%. After this, the APTES combined with the ZnO to form a translucent protective film.

F. MEASUREMENT SYSTEM

A voltage-time (V-T) measurement system [36] was adopted to measure the voltage response of the FPCB pH sensor. Figure 2 shows the connection diagram of the V-T sensing system. A shielded wire was connected to the working electrode, the reference electrode, and the solution ground on the sensor. The six working electrodes were independently connected to the six INAs so that in the same pH solution, simultaneous measurements could be taken for the six sensing nodes. Figure 3 shows the preamplifier PCB, which contained a linear DC-DC conversion circuit. The INA used a commercial LT1167 IC, and the gain was set to one. Output voltage values from the INA circuit are given by Equation (1). The output of the board was connected to a data acquisition (DAQ) device, National Instruments USB-6201 (USA). This converted the sensor response voltages to a digital signal via an internal 16-bit ADC, which has a conversion rate of 50 kHz (10 μs of conversion time). Finally, the response voltage data was processed in LabVIEW software [37].

$$V_{out} = (V_+ - V_-) - V_{ref} \tag{1}$$

where V_+ is the voltage of the LT1167 non-inverting input, V_- is the voltage of the LT1167 inverting input, and V_{ref} is the potential across the reference electrode.

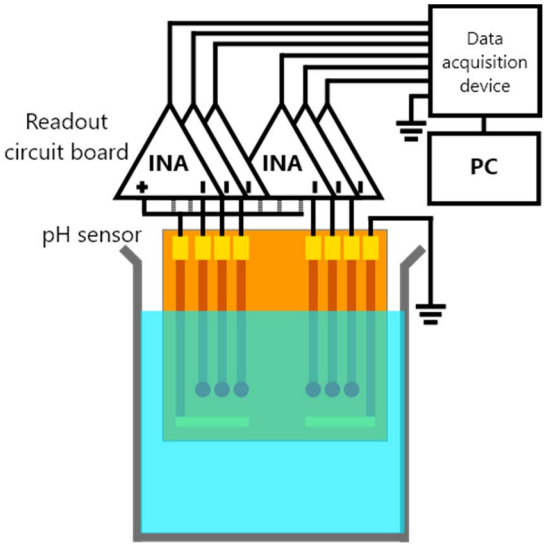

FIGURE 2. Connection diagram of V-T measurement system.

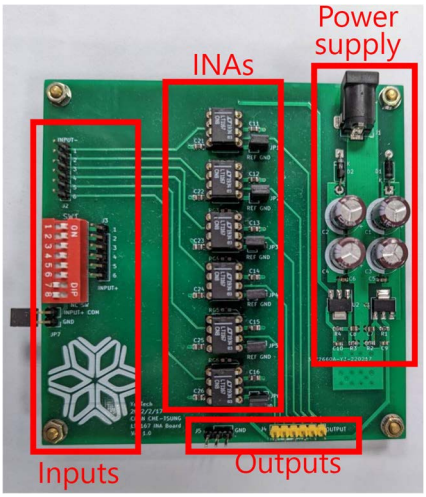

FIGURE 3. LT1167 INA preamplifier PCB.

III. RESULT AND DISCUSSION

A. MORPHOLOGY OF THE ZNO

Field emission scanning electron microscopy (FE-SEM) with a maximum secondary electron image resolution of 1 nm was used to analyze the thickness, and surface quality of RF sputtered ZnO films under different deposition parameters. Figure 4(a) shows there was an average particle size of 30.2 nm (10 sampling points) for 60 minutes of RF sputtering at 60 W RF power, 3 mTorr gas, and with a 9:1 Ar to O_2 gas ratio (sccm). The ZnO sputtered films were solid and dense. Figure 4(b) shows that the average thickness of the ZnO film on the Si substrate was about 155.6 nm.

B. XPS SPECTRUM ANALYSIS OF THE ZNO FILM

The chemical composition of our fabricated ZnO films and the electronic state of the atoms in the material were analyzed using X-ray Photoelectron Spectroscopy (XPS). The XPS measure C 1s (283.7 eV) was used as the reference value and compared with the literature [38]. Figure 5(a) shows the spectrum of Zn 2p, Zn $2p_{3/2}$, and Zn $2p_{1/2}$ has two peaks at 1012.5 eV and 1043.6 eV. The Zn $2p_{3/2}$ peaks exist as metallic zinc in stoichiometric ZnO, while the Zn $2p_{1/2}$ peaks exist as Zn^{2+} ions in the anoxic region. The binding energy difference between these two peaks is about 31.1 eV, showing that zinc exists in the Zn^{2+} oxidation state [39]. Figure 5(b) shows the O 1s spectrum. Three singlets at 529.1 eV, 531.2 eV and 532.0 eV [40]. Calculated in the Gaussian method and the first peak at 529.1 eV is related to the O^{2-} ion in the ZnO structure. The second peak at 531.2 eV is due to O^{2-} ions in Oxygen vacancies of ZnO films [41]. The chemical composition and oxidation state of ZnO sensing films were analyzed. We judge the element ratio [42] in the film by the calculated peak areas of Zn $2p_{3/2}$ = 69842, Zn $2p_{1/2}$ = 21286, and O 1s = 29859. Also, consider the sensitivity factor of Zn $2p_{3/2}$, Zn $2p_{1/2}$, and O 1s were 2.768, 1.384, and 0.733, respectively.

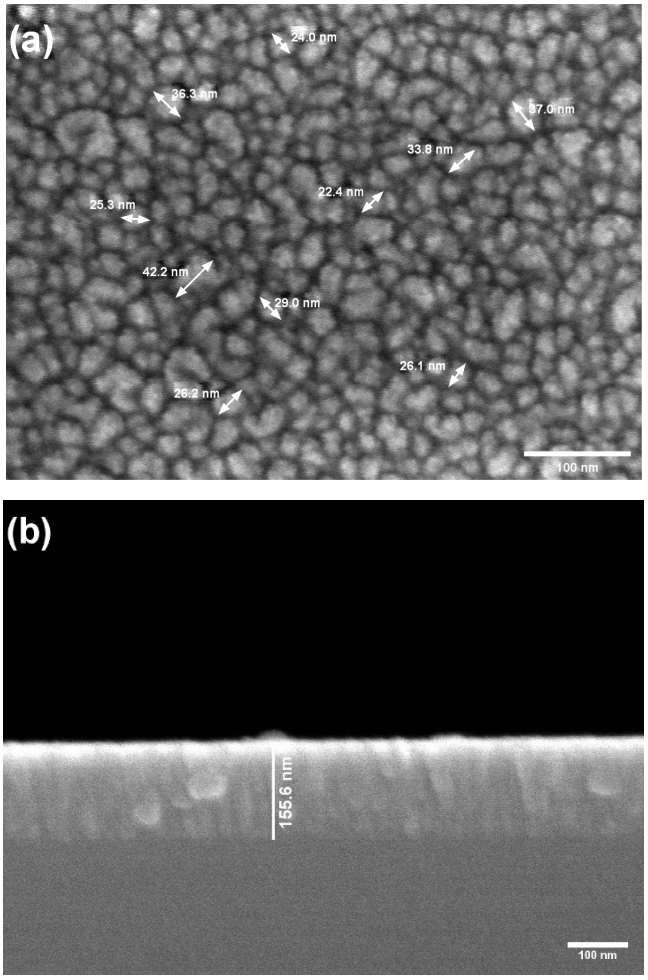

FIGURE 4. Morphologies of the ZnO. (a) top view (b) cross-section view.

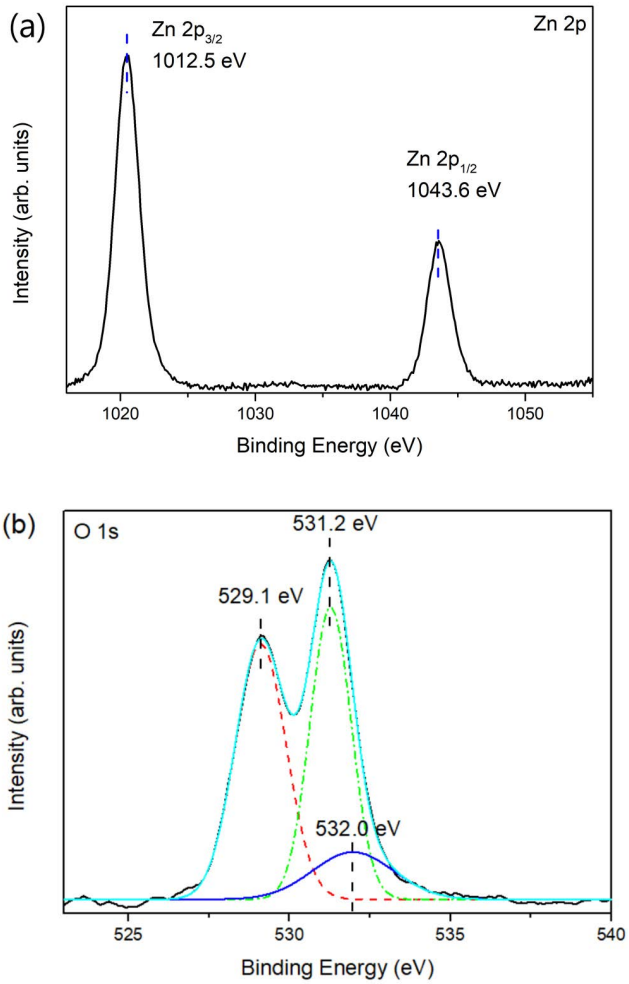

FIGURE 5. The XPS spectrum of ZnO film deposited by R.F. sputter. (a) Zn 2p and (b) O 1s are the high-resolution XPS spectrum.

After multiplying the sensitivity factor, we calculated peak areas of Zn 2p = 40612 and O 1s = 40736. According to XPS analysis results, it can be confirmed that the cationic atoms of zinc have 49.9%, and anionic atoms of O have 50.0%. It can be confirmed that the atomic concentration ratio of zinc to oxygen (Zn/O) is about 1:1.

C. PH SENSING RESULTS

For average sensitivity and linearity measurement, we used pH 2-10 selected as the measurement concentration range, and measurements were taken at pH 2, pH 4, pH 6, pH 8, and pH 10. To prove the sensor has capable of measuring pH in increasing and decreasing methods, we measured the pH 2-10 increasing method and measured the pH 10-2 decreasing method. Therefore, Figure 2 shows the results. The average sensitivity in the increasing method is 37.52 mV/pH, and the linearity is 0.995. Also, the average sensitivity in the decreasing method is 38.56 mV/pH, and the linearity is 0.998. As a result, there was no difference in measurement order. The sensitivity formula can be expressed as formula (2).

$$S = \frac{\Delta V}{R} \tag{2}$$

where ΔV is the change amplitude of the sensor signal, and R is the concentration range of the measurement.

Figure 7 shows the repeatability measurements of the APTES/ZnO FPCB sensor. We measured the pH 6 buffer solution five times after the voltage stabilized. As a result, the sensor maintained a voltage change of 171.38 ± 4.95 mV over five measurements with a relative standard deviation (RSD) of 2.9%. The RSD indicated the performance of the repeatability measurement. RSD can be expressed as Equation (3). S is the 5 times measurements voltage standard deviation. $\bar{X}$ is the 5 times measurements average voltage.

$$RSD = \frac{S}{\bar{X}} \times 100\% \tag{3}$$

D. SELECTIVITY, RESPONSE TIME, AND LIMIT OF DETECTION

The selectivity of ZnO/APTES sensing windows was measured in this study [43]. We performed the selectivity of pH sensors for ion K^+ and Na^+ with respect to the ion H^+ [44]. Also, we take the selectivity experiment into three

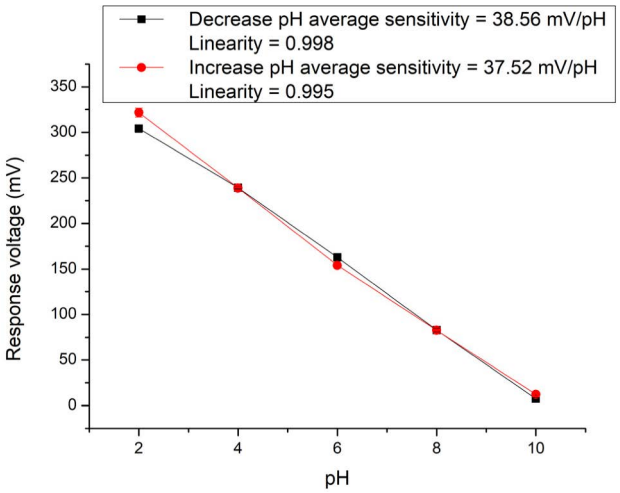

FIGURE 6. Average response voltage of the pH sensor in each pH concentration.

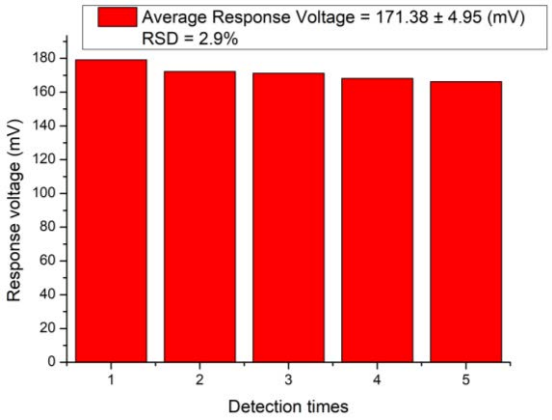

FIGURE 7. Average voltage response of five measurements of pH 6 buffer solution.

parts that analyze pH 4 for acidic situations, pH 7 for the neutral situation, and pH 10 for base situation selectivity performance. First, pH sensors are immersed in pH 7, pH 4, or pH 10 buffer solution, then add NaCl and KCl solution 250 μL in sequence, and observe the voltage change in response. Figure 8 shows the result of the major voltage response when the buffer is immersed and the minor voltage response in 0.1 M NaCl and 0.1 M KCl. The result indicates that the ZnO pH sensor has K^+ and Na^+ activity in acidic, neutral, and base situations. Therefore, the ZnO selectivity performance was just acceptable [45], especially in seawater environments.

The response time indicates the sensor's chemical reaction speed in measurement [44]. Figure 9. shows the response voltage for the pH sensor versus measurement time for pH buffer solution. The sensor response time measured from pH 10 to pH 8, pH 6, pH 4, and pH 2 were 6 seconds, 4 seconds, 4 seconds, and 3 seconds, respectively, where the time calculation is from 0% to 95% of the steady-state

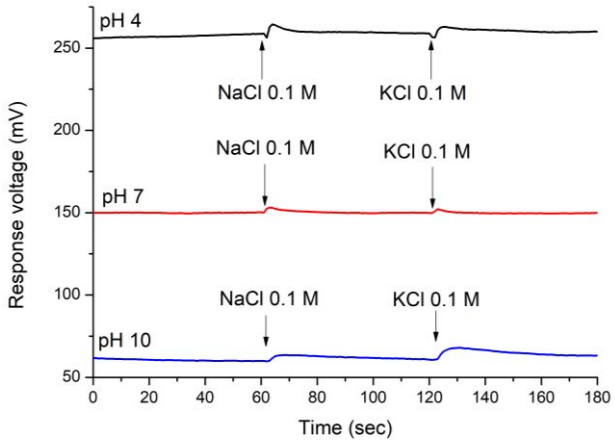

FIGURE 8. pH 4, pH 7, pH 10 response voltages versus interference ion response voltage in selectivity experiment.

response voltage interval. Also, we mentioned the limit of detection was related to APTES/ZnO sensing film strength in the acid and alkaline environment. The acid below pH 2 can permanently damage the sensing film, and the alkaline above pH 10 would accelerate APTES dissolution progress. In that case, the sensor limit of detection is pH 2 – pH 10.

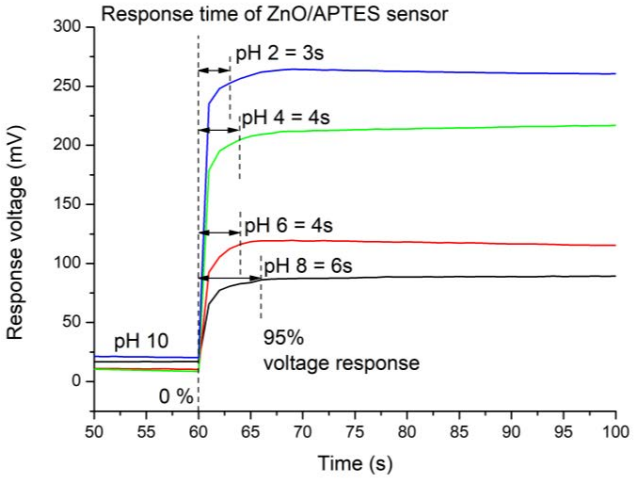

FIGURE 9. The response voltages for the pH sensor versus measurement time.

E. ROLE OF APTES AND THE PH SENSING MECHANISM

The amino silane layer formed by APTES can protect the ZnO in an acid-base solution and increase its chemical stability [46]. The surface of the ZnO can be protonated in acidic buffers as a reaction (4) or deprotonated in alkaline buffers as a reaction (5) [46]. The Nernst equation in (6) [46] indicates that the ZnO surface site density is crucial to its pH sensing ability.

$$ZnO + H^+ \rightarrow ZnOH^+ \tag{4}$$

$$ZnO + 2H_2O \rightarrow Zn(OH)_3^- + H^+ \quad (5)$$

$$E = E_O + \frac{0.059}{n} \log\left(\frac{[ZnOH^+]}{[Zn(OH)_3^-]}\right) + \frac{0.059}{n} pH - E_{ref} \quad (6)$$

where E_O is the standard electrode potential of the ZnO redox electrode, and n is the number of electrons per mole. E_{ref} is the reference electrode potential.

F. FLEXIBILITY TESTING OF THE FPCB SENSOR

Multiple folds have verified the durability of the sensor. Figure 10 (a) shows the sensor in a folded state, and Figure 10 (b) shows the sensor after 100 folds. This produced a visible surface crease but had little effect on the substrate and copper traces. Subsequent testing showed minimal effects on both average sensitivity and linearity. The sensor effectiveness was measured after 0 folds, 50 folds, and 200 folds. Average sensitivity and linearity data are presented in Figure 11.

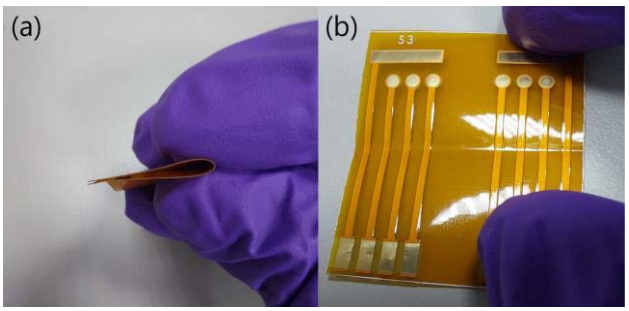

FIGURE 10. Flexible test on the FPCB sensor(a) FPCB in fold state (b) FPCB fold 100 times surface crease.

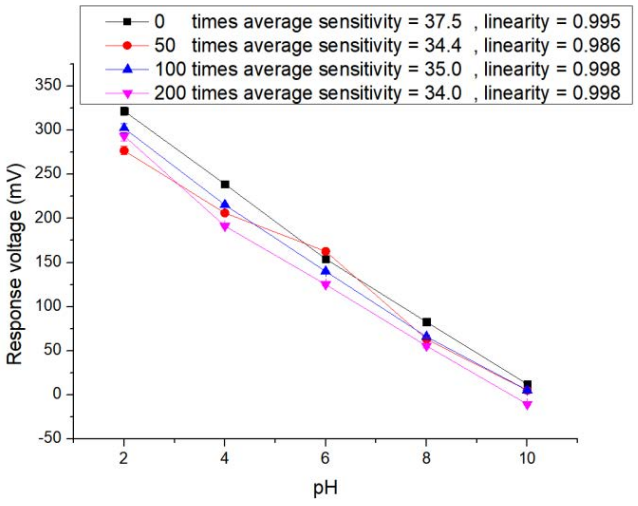

FIGURE 11. Average pH sensitivities of the ZnO/APTES FPCB sensor versus folding times.

G. DRIFT EFFECTS OF THE SENSOR

In this study, we explored the drift of the APTES/ZnO pH sensor. The drift effect represents the long-term measurement stability of the sensor [47]. Before conducting the drift test, a pH 6 solution was used to measure until the response voltage was stable. After completion of the 12-hour drift test, the APTES film remained at the same strength. Figure 12 shows the drift effect of the FPCB sensor with the APTES/ZnO sensing windows. The device was tested in a pH 6 buffer solution for 12 hours. At the fifth hour, the response voltage was 48.0 mV, and at the twelfth hour, the response voltage was −11.5 mV. The drift rate is calculated by subtracting the fifth-hour value from the twelfth hour value and dividing it by the 7 hours difference. In this case, the overall drift rate was 8.5 mV/hour, and the formula is shown below in (7) [48].

$$\textbf{drift rate} = \frac{V_{12th} - V_{5th}}{7} \quad (7)$$

The drift rate is 7 hours of drift voltage. V_{12th} is response voltage at 12 hours. V_{5th} is response voltage at 5 hours.

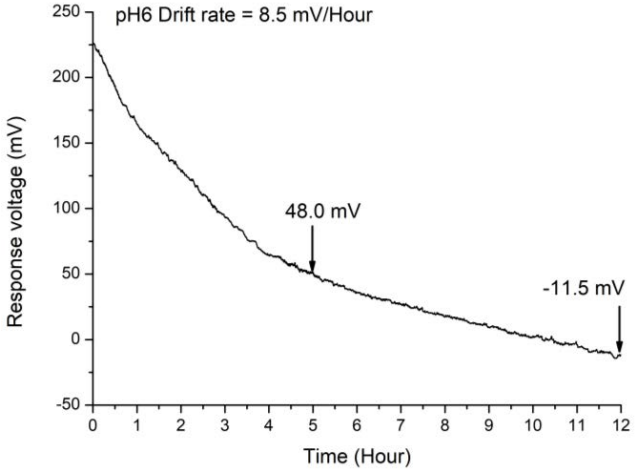

FIGURE 12. Drift effect of the ZnO/APTES FPCB sensor.

H. HYSTERESIS EFFECTS OF THE SENSOR

The hysteresis effect can be known as the sensor's reversibility to test the pH sensor's hysteresis voltage in the hysteresis effect experiment. We prepared pH 7 for a neutral solution, pH 5 for an acid solution, and pH 9 for an alkaline solution. We measured pH 7, pH 5, pH 7, pH 9, and pH 7 sequentially in the forward cycle and measured pH 7, pH 9, pH 7, pH 5, and pH 7 sequentially in the reverse process. Then, the measuring sensor responds to changes in voltage under different pH cycles. Eventually, the final response voltage of the sensor and the initial response voltage will shift, which is called hysteresis voltage [48] between measuring the next concentration. Wait 2 minutes until the voltage is stable, while each pH concentration responded for about 60 seconds. Figure 13(a) depicts the hysteresis effect curve in the forward cycle of the APTES/ZnO FPCB sensing film. The average output voltages for the first and final concentrations were 104.1 mV and 102.0 mV, respectively, and the forward cycling hysteresis voltage was 2.11 mV. Figure 13(b) depicts the hysteresis curve of the reverse cycle measurement of the

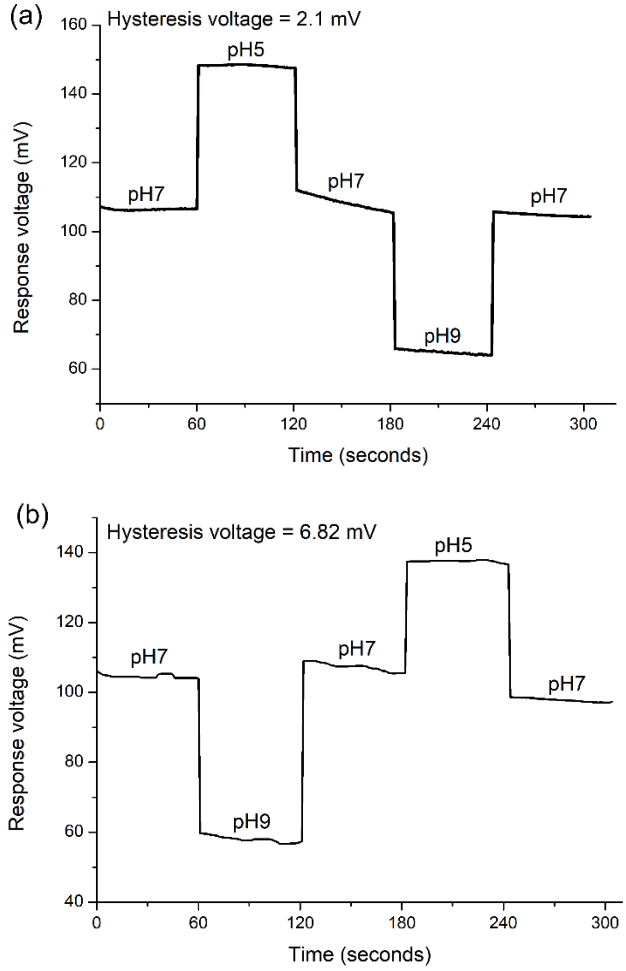

FIGURE 13. Hysteresis voltages of the ZnO sensor by using the V-T measurement system, (a) the forward cycle measurement, (b) the reverse cycle measurement.

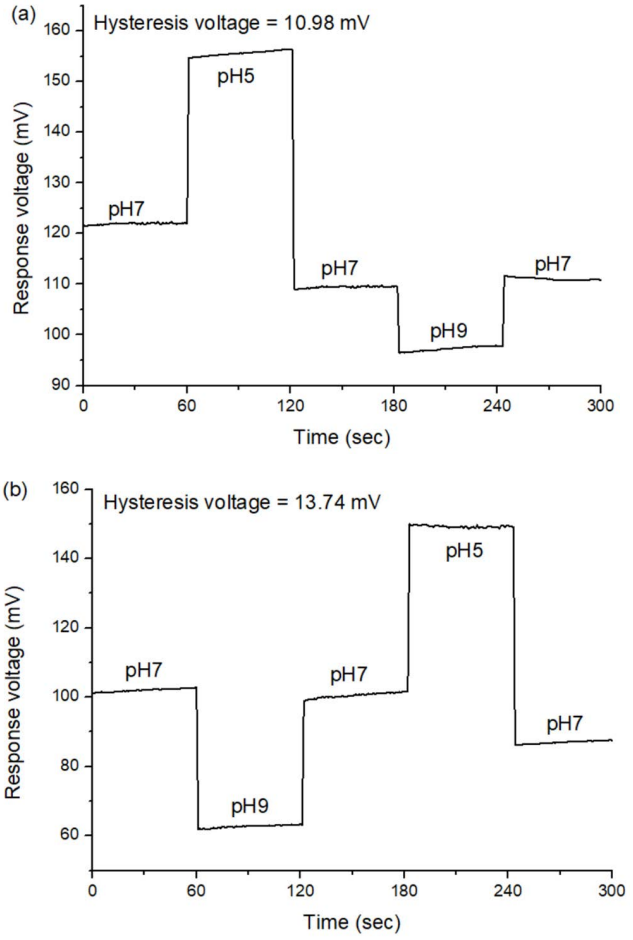

FIGURE 14. Hysteresis voltages of the bare ZnO sensor by using the V-T measurement system, (a) the forward cycle measurement, (b) the reverse cycle measurement.

same sensor. The average output voltages of the first and final concentrations are 102.10 mV and 95.28 mV, respectively, and their reverse cycle hysteresis voltage is 6.82 mV.

We measured the bare ZnO pH sensor hysteresis effect to prove that APTES film can against ZnO damage from an acidic solution. Figure 14(a) shows the response voltage of the forward cycle, and Figure 14(b) shows the response voltage of the reverse cycle measurement. Without APTES protection, the ZnO film will be depleted, and the hysteresis voltage will rise after the pH 5 acid solution is measured. Hence, the forward and reverse cycle hysteresis voltages were 10.98 mV and 13.74 mV, respectively. Hysteresis voltage of bare ZnO sensor is much higher than with APTES-protected sensors, which can prove the protective effect of APTES on zinc oxide.

I. COMPARISONS OF THE ZNO PH SENSOR BASED ON DIFFERENT STRUCTURE

Table 3 shows the comparisons of the ZnO pH sensors. In this study, we proposed sputtering ZnO film pH sensors with APTES, which had the best voltage sensitivity and linearity compared with sputtering ZnO film in

TABLE 3. Comparisons of different ZnO pH sensors sensing characteristics.

Electrode	Fabrication method	Average sensitivity (mV/pH)	Linearity	Linear Range (pH)	Ref.
ZnO Film /APTES	Sputtering	37.5	0.995	2-10	This work
ZnO NR	Low-temp method	28.4	0.980	4-12	[17] 2009
AZO Film	Sputtering	24.3	0.980	7-11	[49] 2011
ZnO NW	CVD	36.6	N/A	4-9	[21] 2015
ZnO NW /APTES	CVD	43.2	N/A	2-9	[21] 2015
Optical fiber Ag	Hydrogel coating	N/A	N/A	1-12	[53] 2018
ZnO Film	Sputtering	34.8	0.992	4-10	[50] 2019
ZnO Film	Sputtering	31.8	0.893	4-12	[51] 2020
TaO_x/Ta Film	Sputtering	61.2	0.999	2-12	[52] 2022

References [49], [50], [51]. Reference [17] shows ZnO nanorod without APTES modified ZnO film. Since APTES was modified, our measurement concentration range includes pH 2-10. Also, compared to recent ZnO with APTES research [21], the sensitivity without APTES was 36.6 mV/pH and with APTES was 43.2 mV/pH. Because of the nanostructure, the voltage sensitivity was slightly better than our work. Meanwhile, compared with other materials studied, such as the Ta pH sensor [52], although it has slightly better performance, ZnO is more advantageous in terms of cost. Compared with the SPR/LSPR fiber-optic pH sensor [53], the traditional thin-film sensing method also has essential advantages of low cost and intuitive measurement.

IV. CONCLUSION

In this study, a dense ZnO layer was successfully sputtered on an FPCB with an ENIG layer to produce a pH sensor with good sensitivity. Applying an APTES coating on the ZnO film improved film resistance in an acidic solution. Appropriate APTES layers can be used to coat the ZnO thin films and prevent degradation in pH 2 solution. Characteristics of the device were measured, including time drift, hysteresis effects, and repeatability. These showed that FPCB could be an excellent electrochemical sensor substrate. This study's APTES/ZnO FPCB pH sensor has an average sensitivity of 37.52 mV/pH and linearity of 0.995.

REFERENCES

[1] A. Safavi and M. Bagheri, "Novel optical pH sensor for high and low pH values," *Sens. Actuators B, Chem.*, vol. 90, nos. 1–3, pp. 143–150, Apr. 2003.

[2] V. S. Chaudhary, D. Kumar, G. P. Mishra, S. Sharma, and S. Kumar, "Plasmonic biosensor with gold and titanium dioxide immobilized on photonic crystal fiber for blood composition detection," *IEEE Sensors J.*, vol. 22, no. 9, pp. 8474–8481, May 2022.

[3] V. S. Chaudhary, D. Kumar, and S. Kumar, "Gold-immobilized photonic crystal fiber-based SPR biosensor for detection of malaria disease in human body," *IEEE Sensors J.*, vol. 21, no. 16, pp. 17800–17807, Aug. 2021.

[4] V. S. Chaudhary, D. Kumar, and S. Kumar, "SPR-assisted photonic crystal fiber-based dual-wavelength single polarizing filter with improved performance," *IEEE Trans. Plasma Sci.*, vol. 49, no. 12, pp. 3803–3810, Dec. 2021.

[5] G. P. Mishra, D. Kumar, V. S. Chaudhary, and S. Kumar, "Design and sensitivity improvement of microstructured-core photonic crystal fiber based sensor for methane and hydrogen fluoride detection," *IEEE Sensors J.*, vol. 22, no. 2, pp. 1265–1272, Jan. 2022.

[6] V. S. Chaudhary, D. Kumar, R. Mishra, and S. Sharma, "Twin core photonic crystal fiber for temperature sensing," *Mater. Today, Proc.*, vol. 33, pp. 2289–2292, Jan. 2020.

[7] G. P. Mishra, D. Kumar, V. S. Chaudhary, and S. Sharma, "Terahertz refractive index sensor with high sensitivity based on two-core photonic crystal fiber," *Microw. Opt. Technol. Lett.*, vol. 63, no. 1, pp. 24–31, 2021.

[8] V. S. Chaudhary and D. Kumar, "TOPAS based porous core photonic crystal fiber for terahertz chemical sensor," *Optik*, vol. 223, Dec. 2020, Art. no. 165562.

[9] Z. Wang, R. Singh, C. Marques, R. Jha, B. Zhang, and S. Kumar, "Taper-in-taper fiber structure-based LSPR sensor for alanine aminotransferase detection," *Opt. Exp.*, vol. 29, no. 26, pp. 43793–43810, Dec. 2021.

[10] M. Li, R. Singh, M. S. Soares, C. Marques, B. Zhang, and S. Kumar, "Convex fiber-tapered seven core fiber-convex fiber (CTC) structure-based biosensor for creatinine detection in aquaculture," *Opt. Exp.*, vol. 30, no. 8, pp. 13898–13914, Apr. 2022.

[11] Y. Wang, G. Zhu, M. Li, R. Singh, C. Marques, R. Min, B. K. Kaushik, B. Zhang, R. Jha, and S. Kuma, "Water pollutants p-cresol detection based on Au-ZnO nanoparticles modified tapered optical fiber," *IEEE Trans. Nanobiosci.*, vol. 20, no. 3, pp. 377–384, Jul. 2021.

[12] A. L. Junior, J. J. Guo, R. Min, A. J. Fernandes, A. Frizera, and C. Marques, "Photonic smart bandage for wound healing assessment," *Photon. Res.*, vol. 9, no. 3, pp. 272–280, Mar. 2021.

[13] F. Vivaldi, D. Santalucia, N. Poma, A. Bonini, P. Salvo, L. D. Noce, B. Melai, A. Kirchhain, V. Kolivoška, R. Sokolová, M. Hromadová, and F. Di Francesco, "A voltammetric pH sensor for food and biological matrices," *Sens. Actuators B, Chem.*, vol. 322, Nov. 2020, Art. no. 128650.

[14] K. Singh, S.-T. Pang, and T.-M. Pan, "Amorphous $ZnSn_xO_y$ fabricated at room-temperature for flexible pH-EGFET sensor," *IEEE Trans. Electron Devices*, vol. 68, no. 2, pp. 793–797, Feb. 2021.

[15] S. K. Arya, S. Saha, J. E. Ramirez-Vick, V. Gupta, S. Bhansali, and S. P. Singh, "Recent advances in ZnO nanostructures and thin films for biosensor applications: Review," *Anal. Chim. Acta*, vol. 737, pp. 1–21, Aug. 2012.

[16] M. Valtiner, S. Borodin, and G. Grundmeier, "Stabilization and acidic dissolution mechanism of single-crystalline ZnO(0001) surfaces in electrolytes studied by *in-situ* AFM imaging and *ex-situ* LEED," *Langmuir*, vol. 24, no. 10, pp. 5350–5358, May 2008.

[17] A. Fulati, S. M. U. Ali, M. Riaz, G. Amin, O. Nur, and M. Willander, "Miniaturized pH sensors based on zinc oxide nanotubes/nanorods," *Sensors*, vol. 9, no. 11, pp. 8911–8923, Nov. 2009.

[18] J.-L. Wang, P.-Y. Yang, T.-Y. Hsieh, C.-C. Hwang, and M.-H. Juang, "pH-sensing characteristics of hydrothermal Al-doped ZnO nanostructures," *J. Nanomater.*, vol. 2013, pp. 1–7, Jan. 2013.

[19] C. F. Lin, C. H. Kao, C. Y. Lin, Y. W. Liu, and C. H. Wang, "The electrical and physical characteristics of Mg-doped ZnO sensing membrane in EIS (electrolyte–insulator–semiconductor) for glucose sensing applications," *Results Phys.*, vol. 16, Mar. 2020, Art. no. 102976.

[20] G. M. Ali, R. H. Dhaher, and A. A. Abdullateef, "pH sensing characteristics of EGFET based on Pd-doped ZnO thin films synthesized by sol-gel method," in *Proc. TAEECE*, vol. 29. Beirut, Lebanon, May 2015, pp. 234–238.

[21] Q. Zhang, W. Liu, C. Sun, H. Zhang, W. Pang, D. Zhang, and X. Duan, "On-chip surface modified nanostructured ZnO as functional pH sensors," *Nanotechnology*, vol. 26, no. 35, Aug. 2015, Art. no. 355202.

[22] S. S. Alias, A. B. Ismail, and A. A. Mohamad, "Effect of pH on ZnO nanoparticle properties synthesized by sol–gel centrifugation," *J. Alloys Compounds*, vol. 499, no. 2, pp. 231–237, Jun. 2010.

[23] T.-M. Pan, C.-H. Lin, and S.-T. Pang, "Structural and sensing characteristics of NiO_x sensing films for extended-gate field-effect transistor pH sensors," *IEEE Sensors J.*, vol. 21, no. 3, pp. 2597–2603, Feb. 2021.

[24] G. Amin, M. H. Asif, A. Zainelabdin, S. Zaman, O. Nur, and M. Willander, "Influence of pH, precursor concentration, growth time, and temperature on the morphology of ZnO nanostructures grown by the hydrothermal method," *J. Nanomater.*, vol. 2011, pp. 1–9, Jan. 2011.

[25] S.-J. Young, Y.-J. Chu, and Y.-L. Chen, "Enhancing pH sensors performance of ZnO nanorods with Au nanoparticles adsorption," *IEEE Sensors J.*, vol. 21, no. 12, pp. 13068–13073, Jun. 2021.

[26] H.-H. Li, C.-E. Yang, C.-C. Kei, C.-Y. Su, W.-S. Dai, J.-K. Tseng, P.-Y. Yang, J.-C. Chou, and H.-C. Cheng, "Coaxial-structured ZnO/silicon nanowires extended-gate field-effect transistor as pH sensor," *Thin Solid Films*, vol. 529, pp. 173–176, Feb. 2013.

[27] J.-C. Chou, J.-T. Chen, Y.-H. Liao, C.-H. Lai, R.-T. Chen, Ya-Li Tsai, C.-Y. Lin, J.-S. Chen, M.-S. Huang, and H.-T. Chou, "Wireless sensing system for flexible arrayed potentiometric sensor based on XBee module," *IEEE Sensors J.*, vol. 16, no. 14, pp. 5588–5595, Jul. 2016.

[28] A. Määttänen, U. Vanamo, P. Ihalainen, P. Pulkkinen, H. Tenhu, J. Bobacka, and J. Peltonen, "A low-cost paper-based inkjet-printed platform for electrochemical analyses," *Sens. Actuators B, Chem.*, vol. 177, pp. 153–162, Feb. 2013.

[29] Y.-M. Fu, J.-C. Pan, K.-L. Tsou, and Y.-T. Cheng, "A flexible WO_3-based pH sensor array for 2-D pH monitoring using CPLoP technique," *IEEE Electron Device Lett.*, vol. 39, no. 6, pp. 881–884, Jun. 2018.

[30] E. Martynenko, W. Zhou, A. Chudnovsky, R. S. Li, and L. Poglitsch, "High cycle fatigue resistance and reliability assessment of flexible printed circuitry," *J. Electron. Packag.*, vol. 124, no. 3, pp. 254–259, Jul. 2002.

[31] J.-C. Chou, S.-J. Yan, Y.-H. Liao, C.-H. Lai, J.-S. Chen, H.-Y. Chen, T.-W. Tseng, and T.-Y. Wu, "Characterization of flexible arrayed pH sensor based on nickel oxide films," *IEEE Sensors J.*, vol. 18, no. 2, pp. 605–612, Jan. 2018.

[32] H. Li, W. Dai, J. Chou, and H. Cheng, "An extended-gate field-effect transistor with low-temperature hydrothermally synthesized SnO_2 nanorods as pH sensor," *IEEE Electron Device Lett.*, vol. 33, no. 10, pp. 1495–1497, Oct. 2012.
[33] W. R. Carmody, "Easily prepared wide range buffer series," *J. Chem. Educ.*, vol. 38, no. 11, pp. 559–560, Nov. 1961.
[34] W. C. Leong, M. Z. Abdullah, and C. Y. Khor, "Application of flexible printed circuit board (FPCB) in personal computer motherboards: Focusing on mechanical performance," *Microelectron. Rel.*, vol. 52, no. 4, pp. 744–756, Apr. 2012.
[35] A. K. S. Kumar, Y. Zhang, D. Li, and R. G. Compton, "A mini-review: How reliable is the drop casting technique?" *Electrochem. Commun.*, vol. 121, Dec. 2020, Art. no. 106867.
[36] C. N. Tsai, J. C. Chou, T. P. Sun, and S. K. Hsiung, "Study on the time-dependent slow response of the tin oxide pH electrode," *IEEE Sensors J.*, vol. 6, no. 5, pp. 1243–1249, Oct. 2006.
[37] Y. H. Liao and J. C. Chou, "Weighted data fusion use for ruthenium dioxide thin film pH array electrodes," *IEEE Sensors J.*, vol. 9, no. 7, pp. 842–848, Jul. 2009.
[38] M. Chen, X. Wang, Y. H. Yu, Z. L. Pei, X. D. Bai, C. Sun, R. F. Huang, and L. S. Wen, "X-ray photoelectron spectroscopy and Auger electron spectroscopy studies of Al-doped ZnO films," *Appl. Surf. Sci.*, vol. 158, nos. 1–2, pp. 134–140, May 2000.
[39] M. N. Islam, T. B. Ghosh, K. L. Chopra, and H. N. Acharya, "XPS and X-ray diffraction studies of aluminum-doped zinc oxide transparent conducting films," *Thin Solid Films*, vol. 280, nos. 1–2, pp. 20–25, Jul. 1996.
[40] P.-T. Hsieh, Y.-C. Chen, K.-S. Kao, and C.-M. Wang, "Luminescence mechanism of ZnO thin film investigated by XPS measurement," *Appl. Phys. A, Solids Surf.*, vol. 90, no. 2, pp. 317–321, Feb. 2008.
[41] J. Wang, Z. Wang, B. Huang, Y. Ma, Y. Liu, X. Qin, X. Zhang, and Y. Dai, "Oxygen vacancy induced band-gap narrowing and enhanced visible light photocatalytic activity of ZnO," *ACS Appl. Mater. Interfaces*, vol. 4, no. 8, pp. 4024–4030, Aug. 2012.
[42] C. Woll, "The chemistry and physics of zinc oxide surfaces," *Prog. Surf. Sci.*, vol. 82, nos. 2–3, pp. 55–120, 2007.
[43] S. Tseng, T. Wu, J. Chou, Y. Liao, C. Lai, J. Chen, and M. Huang, "Research of non-ideal effect and dynamic measurement of the flexible-arrayed chlorine ion sensor," *IEEE Sensors J.*, vol. 16, no. 12, pp. 4683–4690, Jun. 2016.
[44] Y.-H. Liao and J.-C. Chou, "Preparation and characteristics of ruthenium dioxide for pH array sensors with real-time measurement system," *Sens. Actuators B, Chem.*, vol. 128, no. 2, pp. 603–612, Jan. 2008.
[45] A. Wei, L. Pan, and W. Huang, "Recent progress in the ZnO nanostructure-based sensors," *Mater. Sci. Eng. B*, vol. 176, no. 18, pp. 1409–1421, Nov. 2011.
[46] S. Al-Hilli and M. Willander, "The pH response and sensing mechanism of n-type ZnO/electrolyte interfaces," *Sensors*, vol. 9, no. 9, pp. 7445–7480, Sep. 2009.
[47] S.-C. Tseng, T.-Y. Wu, J.-C. Chou, Y.-H. Liao, C.-H. Lai, S.-J. Yan, and T.-W. Tseng, "Investigation of sensitivities and drift effects of the arrayed flexible chloride sensor based on RuO_2/GO at different temperatures," *Sensors*, vol. 18, no. 2, p. 632, Feb. 2018.
[48] J.-C. Chou, T.-Y. Lai, P.-Y. Kuo, C.-H. Lai, Y.-H. Nien, Y.-H. Huang, Y.-Y. Chen, and K.-T. Lee, "Combination of the microfluidic system and NiO uric acid biosensor modified by Ag nanomaterials," *IEEE Access*, vol. 9, pp. 161407–161415, 2021.
[49] J. L. Chiang and C. Y. Kuo, "pH-sensing characteristics and hysteresis effect of AZO/glass extended-gate field-effect transistor," in *Proc. Int. Conf. Electr. Inf. Control Eng.*, Wuhan, China, Apr. 2011, pp. 3434–3437.
[50] S.-J. Young, L.-T. Lai, and W.-L. Tang, "Improving the performance of pH sensors with one-dimensional ZnO nanostructures," *IEEE Sensors J.*, vol. 19, no. 23, pp. 10972–10976, Dec. 2019.
[51] P. Sharma, V. S. Bhati, M. Kumar, R. Sharma, R. Mukhiya, K. Awasthi, and M. Kumar, "Development of ZnO nanostructure film for pH sensing application," *Appl. Phys. A, Solids Surf.*, vol. 126, no. 4, pp. 1–7, Mar. 2020.
[52] T.-M. Pan, C.-H. Lin, and S.-T. Pang, "Structural properties and sensing performance of TaO_x/Ta stacked sensing films for extended-gate field-effect transistor pH sensors," *J. Alloys Compounds*, vol. 903, May 2022, Art. no. 163955.
[53] Y. Zhao, M. Lei, S. X. Liu, and Q. Zhao, "Smart hydrogel-based optical fiber SPR sensor for pH measurements," *Sens. Actuators B, Chem.*, vol. 261, pp. 226–232, May 2018.

PO-HUI YANG (Member, IEEE) received the B.Eng. degree in marine electronics engineering from the National Taiwan Ocean University, in 1993, the M.S. degree in industrial education from the National Taiwan Normal University, in 1995, and the Ph.D. degree from the Institute of Electrical Engineering, National Chung Cheng University, in 2001. From 2001 to 2003, he was an Assistant Professor with the Department of Electronics, Southern Taiwan University of Science and Technology. From 2003 to 2004, he was a High-Performance Digital IC Design Engineer and a Circuit Design Section Manager with the SoC Technology Center (STC), Industrial Technology Research Institute (ITRI), Hsinchu, Taiwan. Afterward, he joined the Department of Electronic Engineering, National Yunlin University of Science and Technology, as an Assistant Professor and an Associate Professor. His research interests include high-speed and low-power CMOS IC design, advanced IC packaging, and low-power biosensor IC design.

CHE-TSUNG CHAN was born in Taichung, Taiwan, in 1998. He received the bachelor's degree from the Department of Electronic Engineering, National Yunlin University of Science and Technology, Yunlin, Taiwan, in 2020. He is currently pursuing the master's degree with the Graduate School of Electronic Engineering, National Yunlin University of Science and Technology. His research interests include analog circuits for biosensors and digital glitch cancellation circuits.

YING-SHENG ZHANG was born in Taoyuan, Taiwan, in 1999. He received the bachelor's degree from the Department of Electronic Engineering, National Yunlin University of Science and Technology, Yunlin, Taiwan, in 2020. He is currently pursuing the master's degree with the Graduate School of Electronic Engineering, National Yunlin University of Science and Technology. His research interests include analog readout circuits and temperature compensation circuits for biosensors measurement systems.